How Chain Length and Charge Affect Surfactant Denaturation of Acyl Coenzyme A Binding Protein (ACBP)

Kell K. Andersen and Daniel E. Otzen*

Interdisciplinary Nanoscience Centre, University of Aarhus, Gustav Wieds Vej 10C, DK−Aarhus C, Denmark, and Department of Life Sciences, University of Aalborg, Sohngaardsholmsvej 49, DK-9000 Aalborg, Denmark

Received: June 13, 2009; Revised Manuscript Received: September 3, 2009

Using intrinsic tryptophan fluorescence, equilibria and kinetics of unfolding of acyl coenzyme A binding protein (ACBP) have been investigated in sodium alkyl sulfate surfactants of different chain length (8−16 carbon atoms) and with different proportions of the nonionic surfactant dodecyl maltoside (DDM). The aim has been to determine how surfactant chain length and micellar charge affect the denaturation mechanism. ACBP denatures in two steps irrespective of surfactant chain length, but with increasing chain length, the potency of the denaturant rises more rapidly than the critical micelle concentration (cmc) declines. Increasing proportions of DDM, which significantly reduce the amount of monomeric sodium dodecyl sulfate (SDS), make the first denaturation step occur at lower concentrations but weaken and eventually remove the second denaturation step. The logarithm of the unfolding rate constants increases linearly with denaturant concentration below the cmc but declines at higher concentrations. Both shortening chain length and decreasing micellar charge reduce the overall kinetics of unfolding and makes the dependence of unfolding rate constants on surfactant concentration more complex. This behavior contrasts with the simplicity of unfolding in chemical denaturants and highlights the changing properties of surfactant micelles. We suggest that the transition from spherical to more elongated micelles leads to inhibition of unfolding kinetics, while weaker binding sites may cause a subsequent rise in unfolding rate constants at higher surfactant concentrations. We propose that shifting micellar binding sites on globular proteins such as ACBP, as opposed to the predefined binding sites on membrane protein surfaces, may lead to nonlinear correlations between activation unfolding energies and SDS mole fraction.

Introduction

Protein−surfactant interactions have been studied ever since the 1940s.[1] Protein−surfactant interactions are today of great value for the performance of the detergency industry, whose total annual revenues are around $17 billion, of which industrial enzymes account for roughly 5%. From a fundamental point of view, protein−surfactant interactions also provide a fascinating glimpse into the many different types of protein conformations that can be induced by surfactant monomers and micelles. These effects are rooted in two properties: First, ionic surfactants' high affinity for protein surfaces, derived from a combination of electrostatic and hydrophobic binding interactions. Second, a high denaturing potency due to their head groups' high charge density, that leads to strong electrostatic repulsion and consequent expansion and denaturation when sufficient numbers of surfactant have accumulated on the protein surface.[2] All this means that anionic surfactants such as sodium dodecyl sulfate are active at low millimolar concentrations, in contrast to the molar concentration range required for chemical denaturants such as guanidinium chloride (GdmCl). Further, the mechanism of denaturation by surfactants is fundamentally different from chemical denaturants; it proceeds much more rapidly, shows complex concentration dependence and has identifiable initial binding sites,[3] leading to denatured conformations that differ substantially from those attained in chemical denaturants.

Most studies have focused on only single component systems such as the anionic surfactant sodium dodecyl sulfate (SDS), however the surfactants used in industry are polydisperse and are mixtures of different chain lengths. Insight into the interactions of proteins and surfactants with different chain lengths is thus important. In addition, most detergent products include both ionic and nonionic surfactants. Nonionic surfactants have significantly lower critical micelle concentrations (cmcs) than ionic surfactants of the same chain length, due to the lack of repulsive headgroup charges. Therefore, besides reducing charge density, mixtures of nonionic and ionic surfactants have significantly lower cmc values than pure ionic surfactants. This effectively removes the concentration range window in which ionic surfactants can act as monomers on proteins and makes micelles the only major surfactant component. If the surfactant monomer is the active component, as has been proposed in some cases,[4] such mixed micelle systems can strongly reduce protein−surfactant interactions and weaken the denaturing effects of surfactants.[5] Nevertheless, surfactant micelles are also strongly denaturing, as exploited in conventional SDS-PAGE. Thus, the use of mixed micelles may shed further light on the relative importance of monomers and micelles in protein−surfactant interactions. However, to our knowledge, only a few studies have been dedicated to the interactions of such mixed micelles with proteins, and these have mainly been devoted to static structural studies.[6−8]

In this paper, we therefore investigate the effect of chain length and the mixing of ionic and nonionic surfactants on denaturation potency against proteins. As model systems, we use the 4-helical bundle protein acyl coenzyme A binding protein (ACBP), an 89-residue protein without disulfides or

* To whom correspondence should be addressed. Tel.: + 45 89 42 50 46. Fax: + 45 86 12 31 78. E-mail: dao@inano.dk.

10.1021/jp905553h CCC: $40.75
Published on Web 09/29/2009

cofactors. By virtue of its small size and simple composition, ACBP has already been used for numerous folding studies.[9−11] We have previously studied the surfactant-induced denaturation of proteins with different secondary structure composition, including all-β,[12] mixed $\alpha-\beta$,[3,13,14] and all-α with prosthetic cofactors.[15] This was motivated by the observation that β-rich proteins generally show increased resistance to surfactant denaturation, while α-rich proteins are more prone to surfactant denaturation.[16] ACBP provides an opportunity to expand these studies to include an α-helix protein without cofactors. Furthermore, the rapid unfolding kinetics of ACBP in SDS and other alkyl sulfates allows us to investigate the interactions with surfactants within a reasonable time window.

We have recently described the interaction of ACBP with SDS using a combination of spectroscopy, calorimetry, capillary electrophoresis, and SAXS.[17] This study has given us detailed insight into the stepwise denaturation of ACBP by submicellar concentrations of SDS. At low SDS concentrations, ACBP binds 1−3 SDS molecules that do not significantly perturb the native structure. In the next step, 16 SDS molecules are bound as a decorated micellar structure, leading to ACBP denaturation and concomitant formation of ACBP dimers. Further uptake of SDS to a total of 42 SDS molecules occurs in an additional transition that involves additional growth of the micellar aggregate. Finally, at SDS concentrations above the cmc, ACBP associates with bulk micelles to form a complex which it has not been possible to characterize in the same detail.

We find that shorter alkyl chains lead to dramatically slower denaturation kinetics in addition to the expected reduction in binding affinity. Interestingly, both a reduction in charge density and shorter chain length lead to more complex unfolding kinetics as well as reducing unfolding rates. This suggests that electrostatics and hydrophobic interactions play similar roles in the denaturation process. Furthermore, there is no significant correlation between the thermodynamic or kinetic stability of ACBP toward unfolding in chemical denaturants versus that in surfactants, highlighting a fundamental difference in the mechanism of unfolding employed by the two classes of denaturants.

Methods and Materials

Materials. Tris(hydroxymethyl)aminomethane (Tris) and sodium dodecyl sulfate (SDS) were from AppliChem (Darmstadt, Germany). Pyrene was from Sigma-Aldrich (St. Louis, MO). N-dodecyl-β-D-maltoside (DDM) was from Calbiochem (San Diego, CA). Sodium *n*-octyl-, decyl-, hexadecyl-, and tetradecyl-sulfate were from Lancaster synthesis. All chemicals were of molecular biology grade. Native ACBP was prepared as described,[18] and ACBP mutants were a kind gift from Flemming M. Poulsen.

Spectroscopic Measurements. All experiments were conducted in 10 mM Tris pH 8.0 at 25 °C using 2 μM ACBP unless otherwise stated. Solutions were left to equilibrate in surfactant at 25 °C for at least 30 min before recording spectra. All spectra were recorded as the average of three emission scans in a 10 mm quartz cuvette (Hellma) with a slit width of 10 nm and a scanning speed of 200 nm/min.

Tryptophan Fluorescence. ACBP's two tryptophan residues (Trp55 and Trp58) in helix 3 are good intrinsic probes of the tertiary structure. Steady-state fluorescence measurements were performed on a LS-55 luminescence spectrometer (Perkin-Elmer Instruments, UK), using slit widths of 10 nm, an excitation wavelength of 295 nm, and recording the emission between 310 and 400 nm.

Pyrene Interactions. Pyrene is a very hydrophobic molecule, whose very low solubility in water (2−3 μM) drives it to partition into available hydrophobic phases such as micelles or surfactant molecule clusters on the protein surface. The fluorescence emission spectrum of pyrene is sensitive to the polarity of the microenvironment.[19] Thus the ratio between pyrene emission at 372.5 and 383.5 nm (I_3/I_1) makes it possible to determine whether pyrene is in a hydrophilic environment (I_3/I_1 ratio $\sim$ 0.65), a hydrophobic environment such as the interior of a micelle (I_3/I_1 ratio $\sim$ 0.95) or micellar clusters of surfactant on the protein surface (I_3/I_1 values between 0.65 and 0.95). A stock solution of 200 μM pyrene in ethanol was made and added to the surfactant samples to a final concentration of 1 μM. Pyrene was excited at 335 nm, and emission between 350 and 440 nm was monitored. Excitation/emission slit widths of 5/3.5 nm were used.

Acridine Orange Fluorescence. A stock solution of 5 mM acridine orange in ethanol was diluted to 20 μM in the the presence of different total concentrations of 1 SDS:3 DDM (mole:mole). Excitation was at 420 nm, and emission at 526 nm using 5 nm slit widths.

Stopped-Flow Unfolding Kinetics. Unfolding kinetics were studied on a SX18MV stopped-flow microanalyzer (Applied Photophysics, Leatherhead, UK) in a thermostatically controlled sample-handling unit. ACBP and surfactant solution were mixed in a volume ratio 1:10 to a final protein concentration of 2 μM, samples were excited at 280 nm, and the emission above 320 nm was monitored using a cutoff filter. The observed kinetics were satisfactorily fitted to single exponential functions. In a few instances at low surfactant concentrations, inclusion of a second exponential improved the quality of the fit; however, this relaxation phase did not appear consistently and constituted less than 10% of the total amplitude, so it was not included in the subsequent analysis.

Two-State Unfolding. Submicellar denaturation by alkyl sulfates and mixed micelles was analyzed empirically according to a two-state model for unfolding from the native to the denatured state:[20]

$$F = \frac{F_{\text{end}} + F_{\text{start}} 10^{(-m([\text{surf}]-[\text{surf}]^{50\%})}}{1 + 10^{(-m([\text{surf}]-[\text{surf}]^{50\%})}} \quad (1)$$

where F is fluorescence emission intensity, F_{start} and F_{end} are the start and end levels of fluorescence, [surf] is the surfactant concentration, $[\text{surf}]^{50\%}$ is the midpoint concentration of denaturation, and m is a parameter describing the general sensitivity of unfolding to SDS concentration. This equation is based on the unfolding of proteins in chemical denaturants, and the assumptions underlying the equation are not necessarily valid for unfolding in surfactant. Equation 1 is only used for comparative purposes to obtain values of $[\text{surf}]^{50\%}$ and m.

Electrostatic Potential. Electrostatic potential was calculated and visualized as described[21] using the pdb file 1hb6.

Results and Discussion

Equilibrium Denaturation of ACBP in Alkyl Sulfates Shows Similar Steps but Different Denaturation Potency. We start our investigation by comparing the denaturing potency of alkyl sulfates of chain length 8−16 toward ACBP, using the intrinsic probe tryptophan and the extrinsic probe pyrene.

As we previously reported for SDS,[17] all ACBP titrations with alkyl sulfates start with a short baseline region in which no change in the Trp fluorescence emission takes place. Subse-

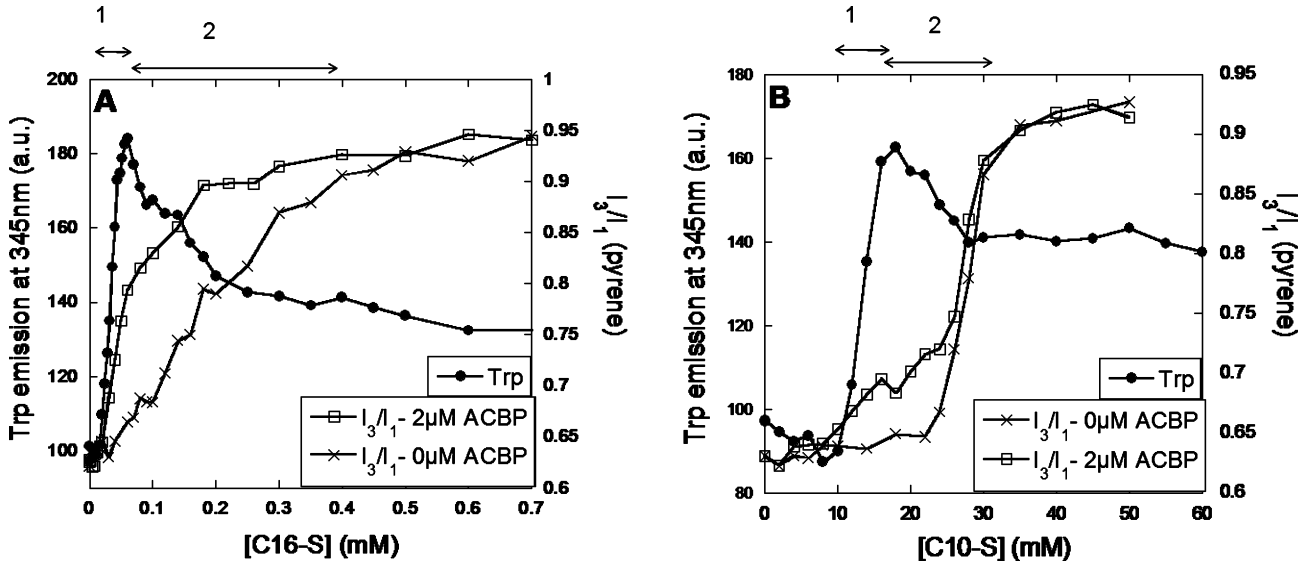

Figure 1. Changes in intrinsic Trp fluorescence emission intensity and extrinsic pyrene emission ratios for ACBP upon titration with (A) C16-sulfate and (B) C10-sulfate. The numbers and arrows refer to transitions 1 and 2.

TABLE 1: Parameters Describing the Equilibrium Denaturation and Kinetics of Denaturation of ACBP in Alkyl Sulfate Surfactants in 10 mM Tris, pH 8.0, and 25°C[i]

chain length	cmc (mM)[a]	Trp denaturation start (mM)[b]	$[surf]^{50\%}$ (mM)[c]	m (mM^{-1})[d]	slope (mM^{-1})[e]	k_{max} (s^{-1})[f]	log k_{obs}^{0mMSDS} [h]
C8	141	60	78.97	0.085	0.0283	12	−2.14
C10	31	10	13.15	0.522	0.157	62	−2.65
C12	6	1.4	1.67	37.021	0.603	175	−1.40
C14	1.06	0.16	0.2	30.753	5.68	[g]	−0.40
C16	0.38	0.019	0.032	68.038	15.6	[g]	−1.03

[a] The concentration of alkyl sulfate at which the pyrene I_3/I_1 ratio in the absence of protein reaches 0.95. [b] The concentration of alkyl sulfate where initial Trp fluorescence start to increase (onset of transition 1; cf. Figure 1). [c] The concentration of surfactant at which half of the ACBP molecules are denatured. Value obtained by fitting eq 1 to Trp fluorescence data describing transition 1 in Figure 1. [d] The cooperativity parameter m obtained using eq 1 and the same data described in footnote c. [e] Slope of the fit in the plot of log k_{obs} vs alkyl sulfate concentration in the insets in Figure 4. [f] The highest measured unfolding rate constant (Figure 4). [g] Not determined because of limited surfactant solubility. [h] The unfolding rate of ACBP in the absence of surfactant calculated by extrapolating linear fits in insets in Figure 4 to 0 mM surfactant. [i] All errors ∼ 5%.

quently, there is a shift in the Trp fluorescence peak maximum (λ_{max}) from ∼342 to ∼346 nm (data not shown), indicating denaturation and increased exposure of the Trp side chain to solvent. This λ_{max} shift is initially accompanied by an increase in fluorescence intensity (representative data for C16-sulfate and C10-sulfate are shown in Figure 1). We refer to this change in fluorescence as transition 1. We showed for SDS that transition 1 is accompanied by changes in both secondary and tertiary structure as well as the formation of a complex consisting of two ACBP molecules with ∼33 SDS molecules, which represents the first major denaturation step.[17] Transition 1 is followed by an intensity decrease to an intermediate level (transition 2) without significant changes in λ_{max}. This transition corresponds to the formation of a single protein−surfactant complex with additional minor rearrangements.[17] Both transitions are highlighted in Figure 1.

The change in pyrene's fluorescence emission ratio I_3/I_1 provides two useful pieces of information. First, in the absence of protein, we can determine the critical micelle concentration (cmc) of the different alkyl sulfates under our buffer conditions (10 mM Tris pH 8.0). The cmc is here defined as the alkyl sulfate concentration where the I_3/I_1 ratio reaches its plateau value of 0.95 (estimated visually with an error of ∼15%). Results are summarized in Table 1. For SDS, this value (6.0 mM) is identical to the value determined by ITC under the same buffer conditions.[17] Second, in the presence of protein, we can follow the formation of surfactant clusters on the protein surface, indicated by increases in the I_3/I_1 ratio well below the cmc. Cluster formation coincides with an increase in tryptophan fluorescence (Figure 1), indicating that surfactant clustering accompanies or leads to denaturation. The cluster I_3/I_1 ratio, which is around 0.8 for C12-, C14-, and C16-sulfate, decreases to ∼0.7 for C10-sulfate and ∼0.65 for C8-sulfate, probably because the short-chain clusters formed are smaller and less hydrophobic than the long-chain ones or simply cannot accommodate pyrene to the same extent. Note that the aggregation number for alkyl sulfates increases from around 24 for C8-sulfate to around 50, 80, and 125 for C10-, C12-, and C14-sulfate.[22]

In order to compare the denaturing potency of the alkyl sulfates, we have analyzed transition 1 using a two-state model typically used to analyze denaturation of proteins in chemical denaturants like GdmCl and urea.[20] We emphasize that we do not imply that the surfactants denature ACBP by the same mechanism as chemical denaturants. Nevertheless, the analysis provides two empirical parameters that describe the denaturing potency of the individual surfactants. The first parameter is the midpoint of denaturation $[surf]^{50\%}$, i.e. the surfactant concentration where half of the protein has lost its native conformation. The second parameter is the cooperativity (the m value) which reflects the concentration range over which the protein goes from the native state to the denatured state (the larger the m value, the narrower the concentration range over which this occurs) and thus refers to the efficiency with which each additional

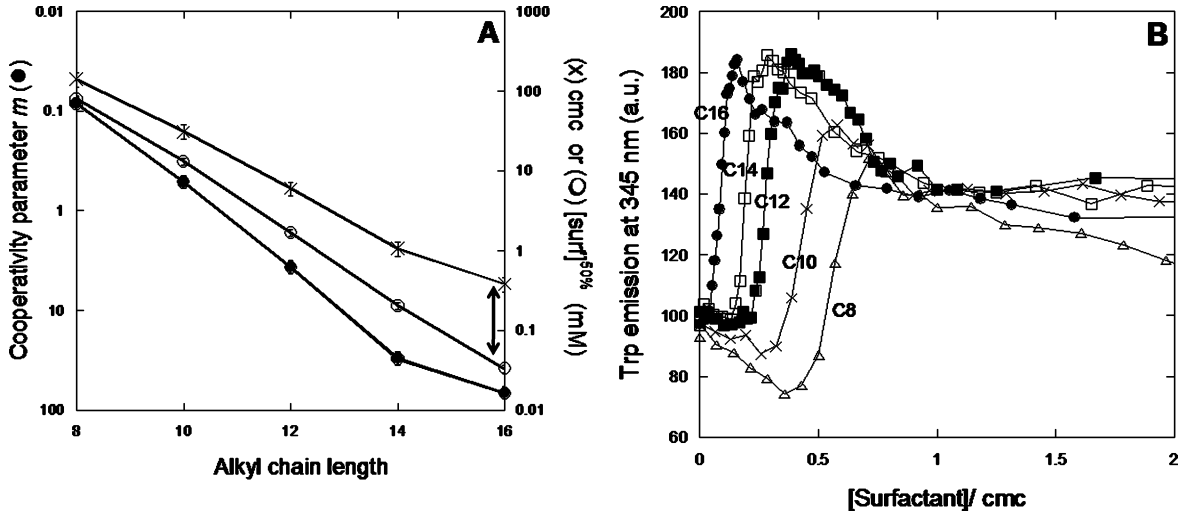

Figure 2. (A) Log plots of cmc and midpoint alkyl sulfate denaturation concentrations $[surf]^{50\%}$ as functions of chain length. The cooperativity of unfolding (m) is also included. Data from Table 1. Errors (~5%) taken from the fits. (B) Trp fluorescence emission intensity of ACBP for C8−C16 alkyl sulfates, where surfactant concentration is normalized relative to cmc. Numbers refer to chain lengths.

surfactant molecule contributes to the denaturation of ACBP. These values are summarized in Table 1.

A log plot of $[surf]^{50\%}$ and cmc versus chain length (Figure 2A) demonstrates that the $[surf]^{50\%}$ is consistently below cmc and the gap between the two values widens with higher chain length. This may also be demonstrated by normalizing alkyl sulfate concentration by its corresponding cmc and plotting Trp titration values for C8−C16-sulfate in one plot (Figure 2B). Thus, the longer the alkyl chain, the more potent the denaturation. Our data reveal that denaturation potency (i.e., the ability to bind to and induce structural changes in the protein) increases more steeply with chain length than the cmc (which reflects the ability of surfactant monomers to associate and form micelles). In other words, the alkyl sulfate chains have slightly higher affinity for the protein than for each other. Consistent with this, the m values also increase more steeply with chain length than cmc and $[surf]^{50\%}$ (Figure 2A), indicating that the surfactants' denaturing efficiency increases faster than the self-association ability. For α-lactalbumin, we also observe denaturation below cmc and increasing divergence from cmc as we increase the chain length.[23]

Equilibrium Denaturation in Mixed Micelles Shows Strong Dependency on Charge Density. Data in the previous section and in our previous work[17] indicates that ACBP denaturation by alkyl sulfates occurs below the cmc. Thus, our data so far only shed light on surfactant monomer (or submicellar) activity toward ACBP. In order to focus on the action of micellar species on ACBP under conditions in which monomers are not expected to play a prominent role, we prepared mixed micelles consisting of SDS and the nonionic surfactant dodecyl maltoside (DDM). DDM (cmc 0.17 mM, i.e. more than 30 fold lower than that of SDS) was chosen due to its prevalence as a model nonionic surfactant and because the alkyl chain has the same length as SDS. Hence, the two surfactants differ only in the properties of the headgroup. In solutions of mixed SDS−DDM micelles, the cmc (i.e., the total concentration of monomeric SDS and DDM) remains around 0.2 mM between 0.75 and 0.25 SDS mole fractions,[24] so we never have more than 0.1−0.2 mM monomeric SDS in our solution. Given that monomeric SDS only starts to denature ACBP around 1.3 mM SDS,[17] we do not expect monomeric SDS to affect ACBP denaturation, which instead will be wholly induced by micelles.

Note that there is no evidence that DDM can interact with ACBP. DDM alone has no effect on ACBP fluorescence, and ACBP does not alter the cmc of DDM (data not shown), due to the general preference of nonionic surfactants for self-association rather than protein binding. However, Trp fluorescence titration with mixed micelles containing 0.25−0.75 mol fractions SDS showed a double-transition denaturation profile similar to that of neat SDS, with a baseline followed by a steep rise in fluorescence and a subsequent decline (Figure 3A). This decline becomes less pronounced at 0.5 and 0.25 mol fractions SDS, possibly because the mixed micelles interact more weakly with ACBP than neat SDS micelles (see below). Just as observed for neat SDS,[17] only the first transition gives rise to a change in the far-UV circular dichroism spectrum (data not shown). We conclude that the first transition is initial denaturation, while no change on secondary structure is observed for the second transition. Thus, micelles and monomers appear to denature ACBP by the same two-state mechanism. A priori, we cannot rule out that the micellar species rearrange and form clusters structures on the surface of ACBP in view of the strong affinity of submicellar alkyl sulfates for the protein surface. Nevertheless, the mechanism of unfolding must be different since the midpoint of denaturation (expressed in terms of SDS concentration and analyzed according to eq 1) shifts to significantly lower values for 0.75, 0.5, and 0.25 mol fraction SDS (Figure 3B). Thus mixed micelles containing SDS are more efficient denaturants than solutions containing only monomeric SDS (and no other surfactants). Nevertheless, the cooperativity of unfolding (also expressed in terms of SDS concentration) only increases slightly from a mole fraction of 1 to 0.75 and declines steeply from 0.5 to 0.25. Thus, high denaturing efficiency requires at least an equimolar presence of SDS in the mixed micelles; at lower SDS mole fractions, the micelles interact significantly more weakly with ACBP. Our kinetic studies provide a detailed extension of this view (see below).

Kinetic studies Reveal Several Modes of Unfolding Which Vary with Chain Length. Studies on the kinetics of protein denaturation by alkyl sulfates provide useful additional information on the denaturation mechanism, as they allow us to identify changes in rate-limiting steps and study changes in denaturation that occur at concentrations well above the cmc.[3,15,21,23,25] We have therefore analyzed the kinetics of unfolding in alkyl sulfate

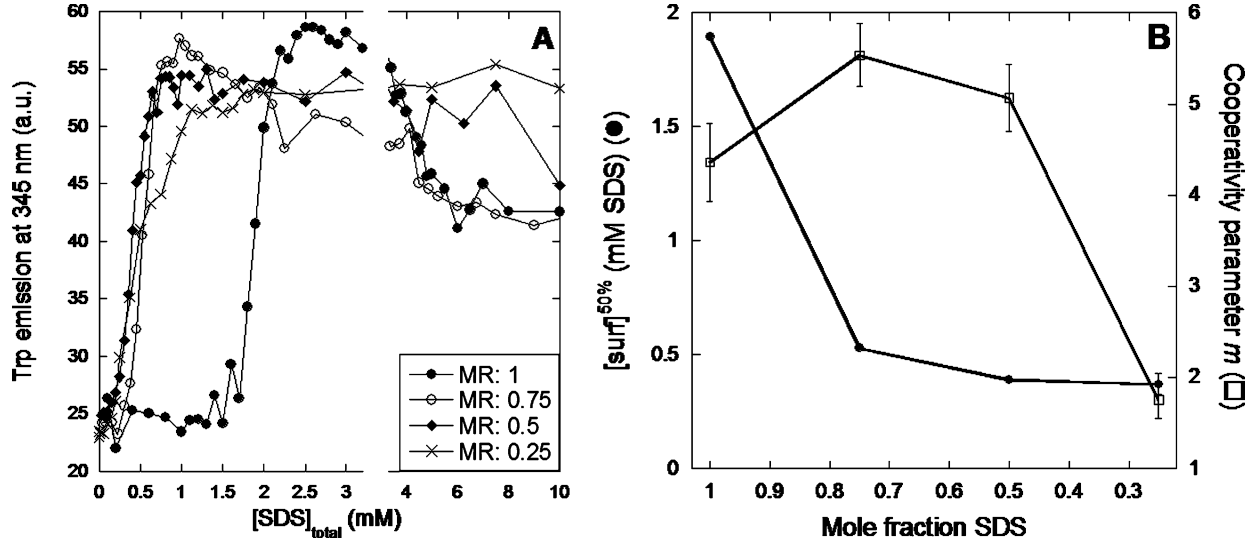

Figure 3. (A) Changes in intrinsic Trp fluorescence emission intensity for ACBP upon titration with mixed micelles at different molar ratios (MR) between SDS and DDM. (B) Midpoint of SDS denaturation $[SDS]^{50\%}$ and the cooperativity (m) plotted as a function of the SDS molar ratio. Errors are taken from fits.

surfactants of different chain lengths as well as mixed micelles. This is carried out by following the time-course of the change in Trp fluorescence emission intensity when ACBP is mixed with surfactants at different concentrations and fitting the data to single exponential curves to obtain the unfolding rate constant k_{obs}.

Plotting log k_{obs} versus alkyl sulfate concentration reveals several characteristic transitions. The first transition starts at the lowest concentrations where unfolding can be detected and continues up to a concentration which very precisely coincides with the cmc. In this sub-cmc region, we observe a linear rise in log k_{obs} for all alkyl sulfates with slope m_{kin} (Figure 4A−D insets). The same type of linear correlation is typically observed for chemical denaturants such as GdmCl but over much larger concentration ranges.[26] The value of log m_{kin} scales linearly with chain length (Figure 5A). The slope of this plot (0.34 ± 0.01) is an indication of how the efficiency of surfactant denaturation capacity grows with the chain length. This value is in absolute terms identical within error to the slope for log cmc versus chain length (-0.33 ± 0.01) (the signs are opposite because m-values are inversely proportional to surfactant concentration; thus, the smaller the concentration increase needed to effect a certain change, the larger the m value). This indicates that hydrophobic interactions stabilize surfactant−protein contacts and surfactant self-assembly to essentially the same degree. The same conclusion was reached from our steady-state measurements (see above).

There are notable differences between denaturation in SDS and GdmCl. First, surfactant denaturation occurs at 50−10.000 fold lower concentrations (depending on the surfactant) than denaturation in GdmCl. Second, when we extrapolate log k_{obs} to 0 M surfactant, we obtain significantly different values in different surfactants (Table 1), varying by 2 orders of magnitude. This may reflect subtle differences in the way the surfactants of different chain length bind to ACBP (despite their overall similarity of interactions). Given that binding is very strong and relatively specific at these low concentrations, it is not unreasonable to expect differences at this level. Furthermore, these rate constants are 10^7-10^9 times faster than the rate of unfolding of ACBP in buffer extrapolated from unfolding rate constants in GdmCl,[27] which again emphasizes fundamental differences between unfolding mechanisms, and the structure of the denatured state, in GdmCl versus surfactant.

Above the cmc, denaturing kinetics evolve differently depending on the chain length. For SDS (Figure 4C), kinetics slowly level off to a plateau value which is reached around 40−60 mM (corresponding to 7−8cmc). At higher concentrations of SDS, unfolding kinetics decrease and reach a plateau at around 300 mM. For C8- and C10-sulfates (Figure 4A and B), kinetics do not increase beyond cmc, instead kinetics slows down to a level around 30−50% of the maximal value. For C8-sulfate this is subsequently followed by a rise (Figure 4A) that is linear in a log−log plot (data not shown). For C14-sulfate (Figure 4D) and C16-sulfate (data not shown), we cannot measure unfolding kinetics much above cmc, due to the surfactants' limited solubility.

C8- and C10-sulfate denaturing kinetics thus differ from SDS-induced unfolding kinetics in that the unfolding kinetics increase above the cmc for SDS while it decreases for C8- and C10-sulfate. This effect may be due to the difference in micelle structure/properties. While SDS forms spherical micelles at relatively low concentrations, a transition to more elongated micelles takes place at high concentrations.[28,29] Romani et al.[30] have recently determined the transition from spherical to elongated micelles (called cmc_2) to occur at a concentration of 50 mM SDS in the absence of buffer. The very dilute buffer we use (10 mM Tris pH 8.0) only reduces the cmc of SDS from 7 mM in water to 6.0 mM in buffer. Assuming that the buffer reduces cmc_2 by the same extent as cmc, we predict a value for cmc_2 around 42 mM in our buffer. This value is quite compatible with our kinetic results, which show that the rate constant for unfolding of ACBP in SDS starts to decline in that concentration range. We have obtained similar results for the unfolding of S6 at low buffer concentrations (Figure 1A in ref 25). This strongly suggests that the appearance of rodlike micelles is responsible for the inhibition of protein unfolding in SDS, simply due to a reduced efficiency of binding and induced conformational changes.

Elongated micelles may also rationalize other literature observations. An interesting study on the unfolding of endoglucanase III (EGIII) in alkyl sulfates altered surfactant monomer concentrations by changing ionic strength.[31] Low ionic strength (with higher cmc and thus higher monomer concentrations) led to faster unfolding in 25 mM SDS, making the authors suggest that monomeric SDS is a major driving force for unfolding. However, it is also possible that the higher ionic

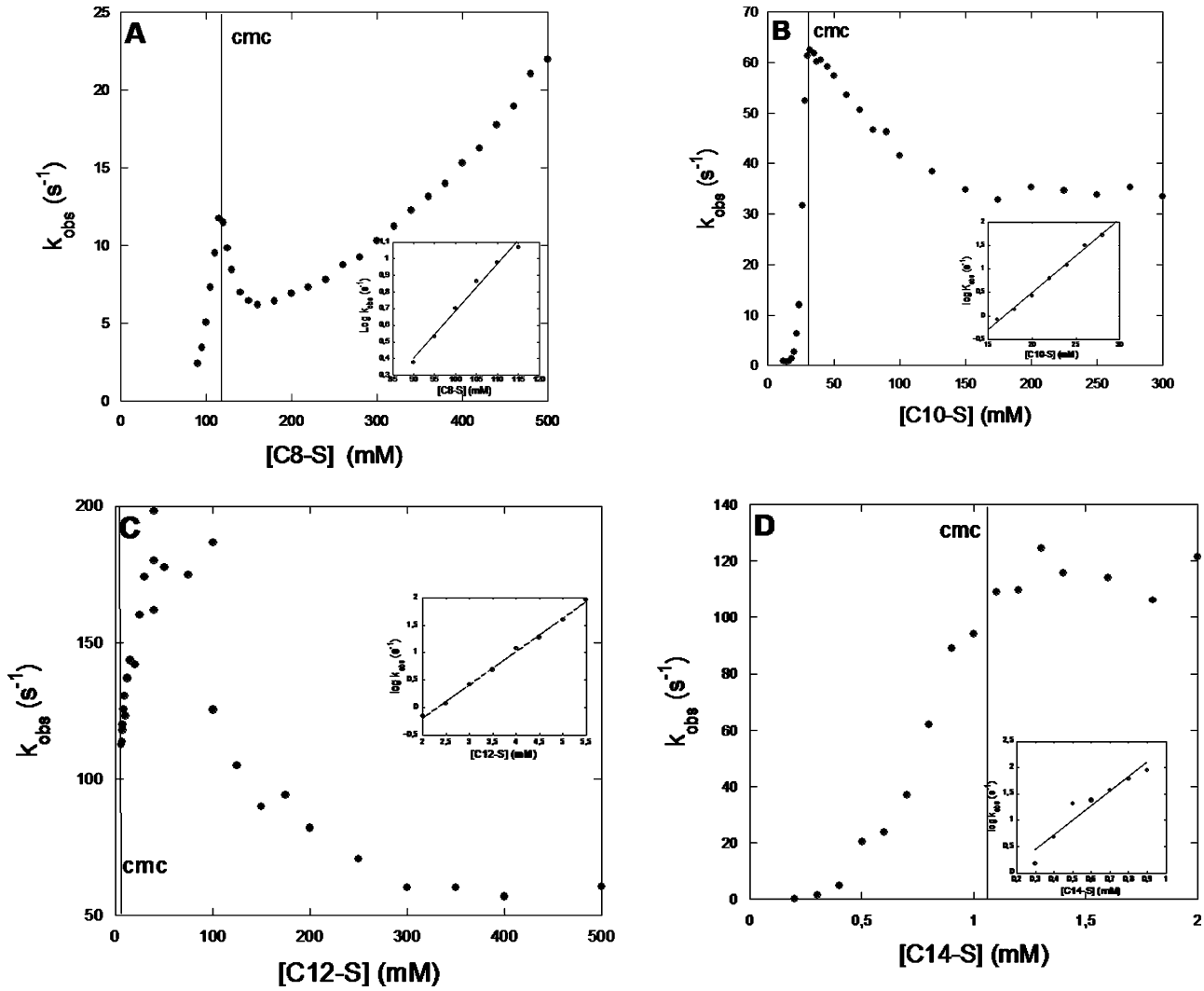

Figure 4. ACBP denaturation kinetics in alkyl sulfates. The unfolding rate constant (k_{obs}) is plotted as function of surfactant concentration, and the cmc is indicated with a vertical line. Insets show the linear dependence of the logarithm of the unfolding rate constant on surfactant concentration below the cmc. Panels A−D refer to alkyl chain lengths of 8, 10, 12, and 14, respectively.

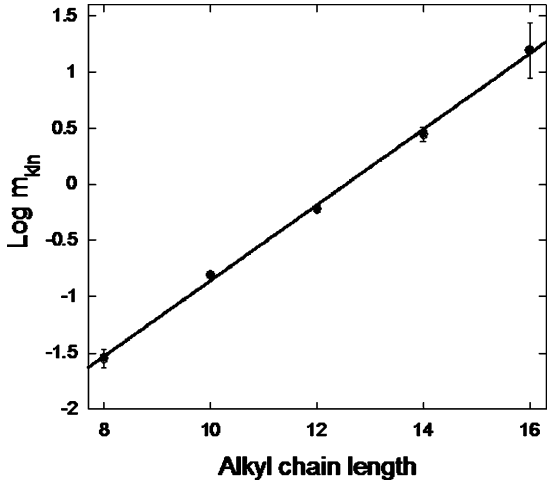

Figure 5. Log of the slope of the fit in Figure 4 insets plotted vs alkyl sulfate chain length. The linear fit has a slope of 0.34 ± 0.01 and an intercept of −4.34 ± 0.25. Errors are taken from fits.

strength induced formation of elongated SDS micelles at 25 mM SDS, and these micelles might lead to reduced rates of unfolding of EGIII, just as we observe for ACBP. The authors also observe that EGIII does not unfold in C8- and C10-sulfates below the cmc, which suggests that micelles, rather than surfactant monomers, are the species that induce EGIII unfolding.

It is unclear whether the power-law rise in k_{obs} observed for C8-sulfate at very high concentrations is related to changes in micellar properties. We have not been able to find any published information about the micellar properties of C8-sulfate at high concentrations and do not obtain any clear indications for rearrangement using acridine orange (data not shown). We have observed a similar power-law rise in k_{obs} for the unfolding of several other proteins at concentrations above ∼200 mM SDS, namely S6,[25] Tnfn3, and TII27.[21] However, the transition to power-law rise is delayed to 300−400 mM SDS in the case of CI2[25] and is completely absent for ACBP in SDS and C10-sulfate. We initially suggested that the power-law rise could be attributed to alterations toward a more elongated micellar structure, but in view of the more recent data presented here and the recent value for cmc_2 provided by Romani et al.,[30] we have to revise that suggestion. Rather, the power-law rise may reflect the presence of additional weak surfactant-binding sites on the protein surface that only rise to prominence at very high surfactant concentrations. This effect may be suppressed by the counteracting influence of other binding sites which inhibit protein unfolding. We should emphasize that all these super-cmc phenomena arise as a result of specific interactions between

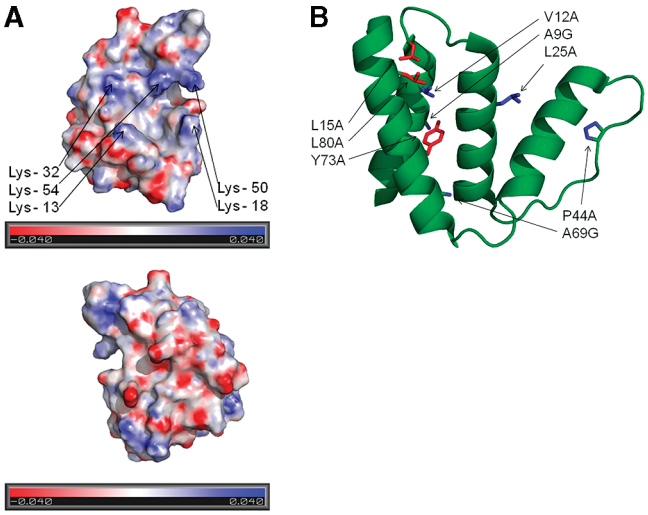

Figure 6. (A) Electrostatic potential of ACBP viewed from two different angles. The five lysines contributing to the positive potential around the ligand binding site are indicated. (B) Cartoon representation of ACBP. The A9G, V12A, L25A, P44A, and A69G mutations are highlighted with blue stick side chains, and the three kinetic outliers L15A, Y73A, and L80A are highlighted with red stick side chains. The pdb file 1HB6 was used and presented in Pymol.

proteins and surfactants which will vary from protein to protein. In dilute Tris buffer, S6 only showed a very modest (ca. 40%) reduction unfolding in SDS (in contrast to the 70% reduction for ACBP), whereas the power-law rise leads to a 4-fold increase in k_{obs} between 250 and 500 mM SDS.[25] In the same concentration range, k_{obs} for CI2 only increases by 20% while k_{obs} for ACBP remains constant.

Mutant Data Suggest Possible Sites of Attack by SDS around the Ligand Binding Site. To obtain an initial estimate of the possible binding sites for SDS on ACBP, we have calculated the electrostatic potential of ACBP (Figure 6A). The electrostatic potential clearly identifies the binding site of acyl-CoA, which consists of both hydrophobic moieties and an anionic (phosphate) tail. The binding site consists of a non-charged (and mainly hydrophobic) crevice surrounded by positively charged residues (blue), of which five are lysines. The side of ACBP opposite to this site contains several negatively charged residues (red). This clear distribution of exposed positive and negatively charged residues will most likely favor electrostatic interactions with anionic SDS around the ligand-binding site.

We next investigated the role that different side chains may play in the ACBP−SDS interaction through an analysis of the SDS-induced unfolding of eight different mutants of ACBP. These mutants, which are based on truncation of hydrophobic side chains distributed randomly within ACBP (shown in Figure 6B), have previously been used to study the folding and unfolding of ACBP in denaturants in order to construct a picture of the transition state for folding and unfolding.[32] Given that the unfolding behavior in GdmCl represents the intrinsic unfolding behavior of ACBP, we can in principle identify specific ACBP−SDS interactions by comparing unfolding data in GdmCl and SDS.[3] The SDS unfolding parameters we use are the midpoints of unfolding transition 1 (Figure 7A) and the rate of unfolding at low SDS concentrations where log k_{obs} depends linearly on SDS concentration (Figure 7B), as summarized in Table 2. These values are then plotted against their GdmCl-based counterparts in Figure 7C and D. The counterpart to $[SDS]^{50\%}$ is the stability of the different mutants (based on equilibrium titration in GdmCl and directly proportional to the midpoint of denaturation in GdmCl). The counterpart to log k_{obs}^{0mMSDS} (i.e., extrapolated to 0 M SDS) is the unfolding rate in GdmCl extrapolated to 0 M GdmCl. In both cases, we observe a clustering of data. SDS data for five of the mutants (A9G, V12A, L25A, P44A, and A69G) correlate well with GdmCl data, whereas three other mutants (L15A, Y73A, and L80A) form a distinct outlier group. This group shows much lower unfolding rate constants in SDS—and a much higher SDS midpoint denaturation—than we would predict based on the linear correlations established by the five mutants in Figure 6C and D. As we have proposed earlier for S6,[3] we would expect that a region of the protein, which is "softened" through initial attack by SDS prior to overall unfolding, would be less sensitive to mutations than regions not bound to SDS before unfolding. This is because such a dynamic region of the protein will not be stabilized by well-defined side-chain interactions. Interestingly, ACBP's first α-helix (residues 4−16) is significantly more dynamic than the other three helices according to hydrogen−deuterium exchange experiments,[33] but this does not translate into a greater degree of sensitivity toward SDS, emphasizing once again a lack of simple correlation between protein stability and denaturation in SDS.

We have considered two other ways to rationalize the specific effects of SDS, namely electrostatics and ligand binding, but do not find clear indications in either case. Let us start with electrostatics: The two β-sandwich structured protein TnfN3 and TII27 showed that although very similar in protein fold, TII27 could be denatured by SDS monomers while TnfN3 showed very little interaction with monomer SDS and was only denatured in the presence of SDS micelles. We correlated the difference in SDS resistance to the difference in electrostatic potential.[21] In the case of ACBP, there is not a distinct separation of the two classes of mutants identified by our kinetic analysis when mapped onto the protein's structure (Figure 6B). Turning to the ligand binding site, we note that the three outlier mutants (L15A, Y73A, and L80A) are all situated fairly closely in space around the ligand binding site. This region shows a positive electrostatic potential, primarily due to the location of five lysines (13, 18, 32, 50, and 54), of which Lys32 and Lys54 directly interact with the 3′ adenosine phosphate group of AcCoA while the pyrophosphate group contacts Lys13.[34] The side opposite the binding site shows large areas of negative electrostatic potential. Due to its positive electrostatic potential, the ligand binding site, and the three outlier mutant side chains, could be the initial site for SDS binding on ACBP. Truncation of side chains in the area where SDS interacts could therefore in principle reduce susceptibility to SDS denaturation. However, we emphasize that this connection is speculative and is unlikely to be the sole reason for the two classes, since the separation between the two proposed classes of mutants on the protein surface is not very distinct. Of the five other mutants, two (A9G and V12A) are in fact close to the ligand binding site, though situated in a different area compared to L15A, Y73A, and L80A.

The significant differences in unfolding kinetics between the eight mutants primarily manifest themselves in the linear plot regions. There is a much smaller variation in the extent to which SDS inhibits unfolding kinetics above the cmc (data not shown). This indicates that the protein conformations induced by SDS at this stage are much less sensitive to specific side chain interactions, probably due to changes in the binding modes at the higher SDS concentrations.

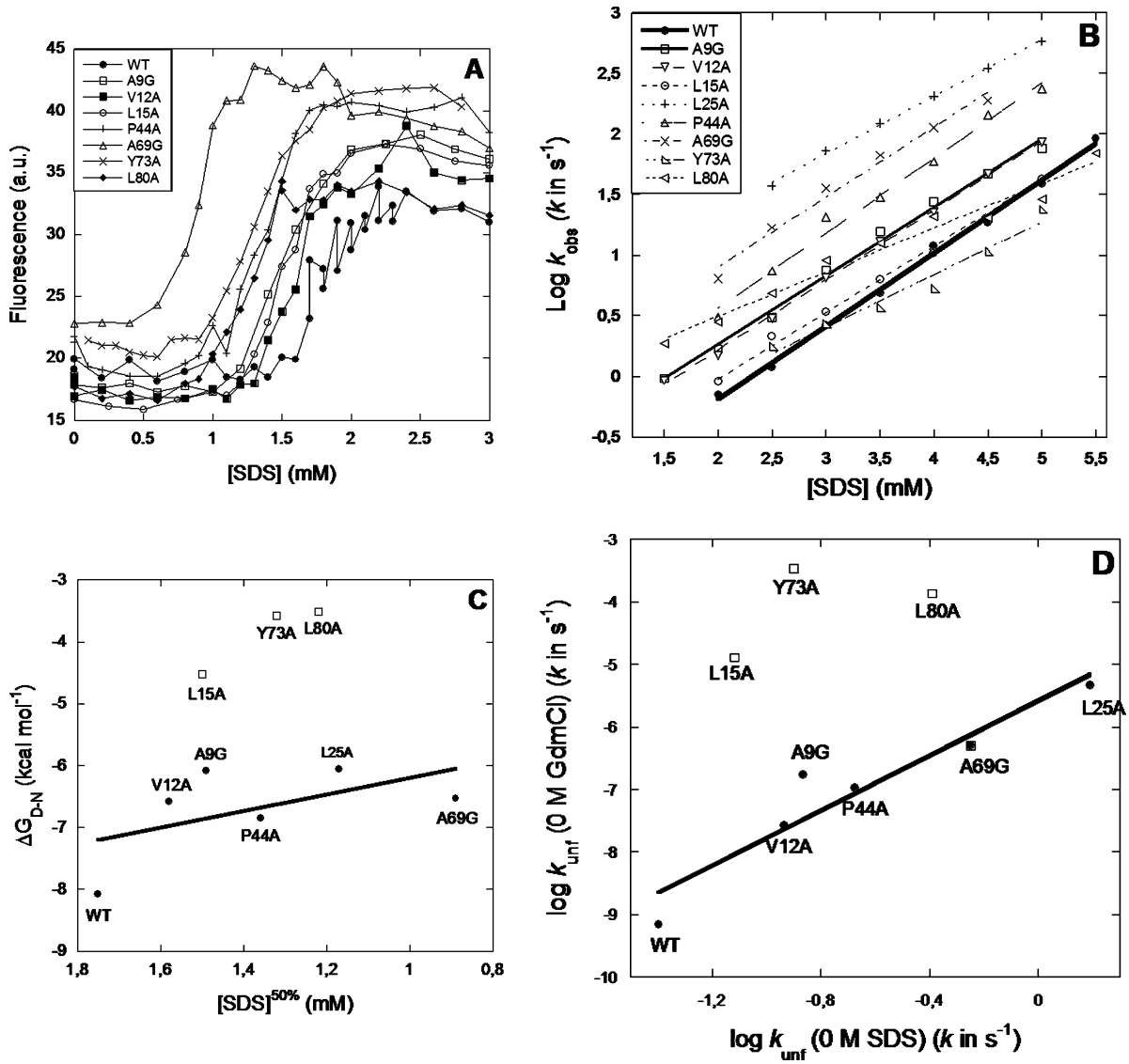

Figure 7. ACBP mutation data. (A) Intrinsic Trp fluorescence as a function of SDS. (B) Denaturation kinetics in the SDS concentration range below the cmc. (C) Free energies of unfolding (ΔG_{D-N}) for different ACBP mutants (obtained from ref 40) plotted against the $[SDS]^{50\%}$. Mutants are grouped into two populations. Wild type (WT) and the mutants A9G, V12A, L25A, P44A, and A69G show a linear correlation, while L15A, Y73A, and L80A diverge from this linearity. (D) Unfolding rates constants in 0 M GdmCl vs unfolding rate constants in 0 M SDS. As in part C, mutants can be classified into two groups. WT and the mutants A9G, V12A, L25A, P44A, and A69G show a linear correlation, while L15A, Y73A, and L80A diverge from this linearity.

TABLE 2: Parameters Describing the Equilibrium Denaturation and Kinetics of Denaturation of ACBP Mutants in SDS[e]

mutant	log $k_{unf}^{0MGdmCl}$ [a]	log k_{unf}^{0mMSDS} [b]	ΔG_{D-N} (kcal mol^{-1})[a]	$[SDS]^{50\%}$ (mM)[c]	slope[d]
WT	−9.16	−1.40	−8.08	1.75	0.60
A9G	−6.76	−0.87	−6.08	1.49	0.56
V12A	−7.58	−0.93	−6.58	1.58	0.58
L15A	−4.89	−1.12	−4.52	1.50	0.55
L80A	−3.87	−0.39	−3.51	1.22	0.43
L25A	−5.33	0.19	−6.06	1.17	0.53
P44A	−6.98	−0.68	−6.85	1.36	0.62
A969G	−6.3	−0.25	−6.53	0.89	0.58
Y73A	−3.47	−0.90	−3.57	1.32	0.43

[a] Data from ref 40. [b] The unfolding rate in the absence of SDS calculated by extrapolating linear fits in Figure 6B to 0 mM SDS. [c] The concentration of surfactant at which half of the mutant molecules are denatured. Value obtained by fitting eq 1 to the Trp fluorescence data describing transition 1 in Figure 6A. [d] Slope of fits in Figure 6B. [e] All data at pH 8.0 and 25°C.

Mixed Micelles Show Similar Unfolding Kinetics As Submicellar SDS and Highlight the Impact of Changing Micellar Compositions. We now describe how mixed micelles of SDS and DDM affect ACBP's unfolding kinetics. Mixed micelles show the same general profile as neat SDS, namely a reasonably linear rise to a plateau level followed by a decrease to another plateau level (Figure 8A). Thus, monomeric SDS is not a prerequisite for the rapid unfolding process that occurs at low surfactant concentrations. However, the SDS concentrations at which the different transitions occur, and the unfolding rate

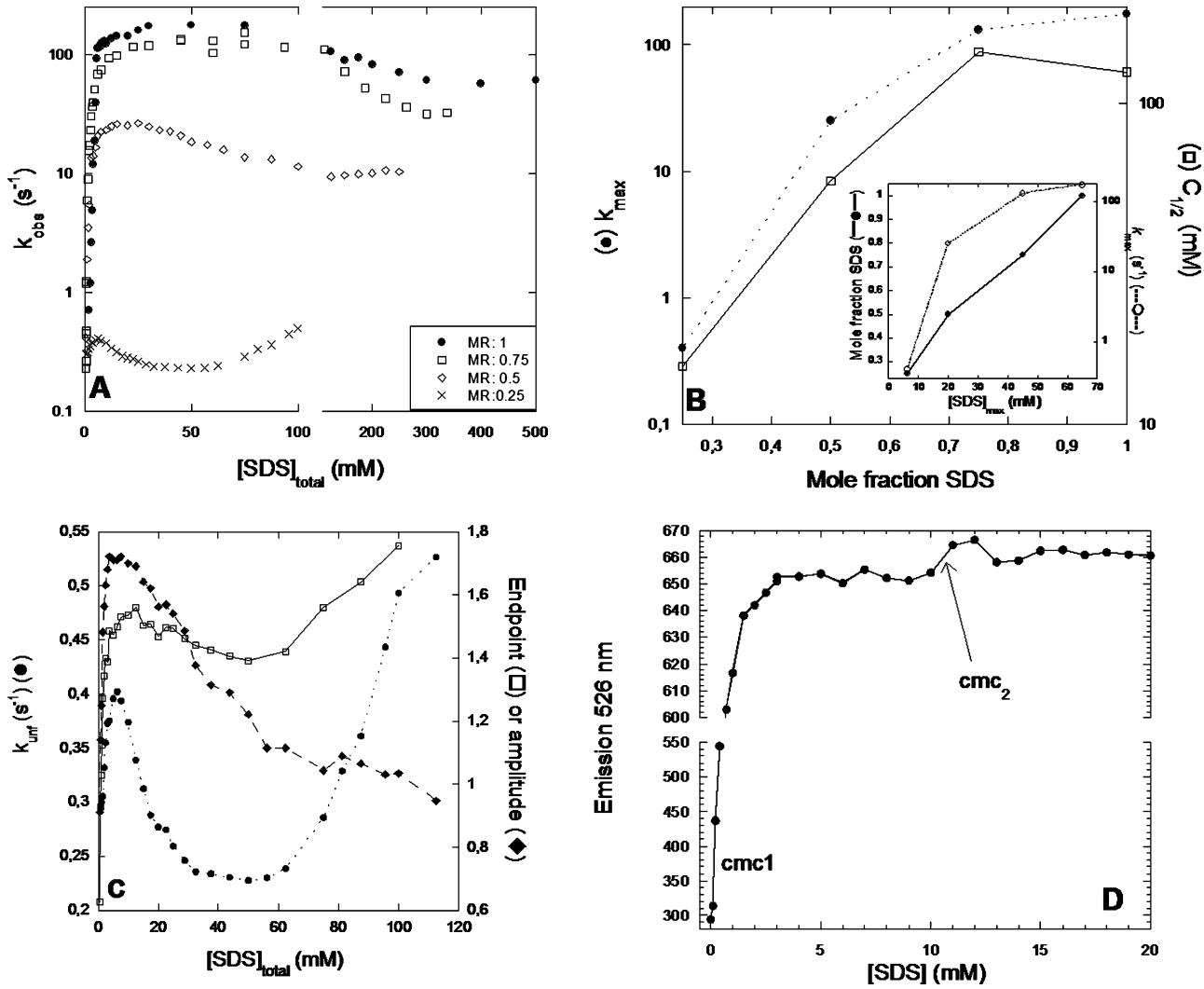

Figure 8. ACBP denaturation kinetics in mixed micelles at different molar ratios (MR) of SDS and DDM. (A) Unfolding kinetics at SDS mole ratios of 0.25−1. Note that k_{obs} is plotted against the total SDS concentration and not the total surfactant concentration. (B) k_{max} and $C_{1/2}$ vs SDS mole ratio. k_{max} is the unfolding rate constant at which kobs is at its highest, and $C_{1/2}$ is the surfactant concentration where k_{obs} is halfway between k_{max} and the plateau level reached at higher concentrations. Values have been derived from data presented in Figure 8A. (inset) SDS concentration where unfolding is fastest (determined from data in panel A) plotted versus mole fraction of SDS. (C) Unfolding kinetics and the associated amplitude and end point at an SDS mole ratio of 0.25. (D) Change in acridine orange fluorescence emission as a function of SDS concentration in mixed micelles with an SDS mole ratio of 0.25.

constants, vary significantly. Both the maximal rate constant of unfolding (k_{max}) and the midpoint of the second transition ($C_{1/2}$) are reasonably constant for 100 and 75% SDS but decline at lower SDS mole fractions (Figure 8B), in the case of k_{max} by more than 2 orders of magnitude. A similar correlation is obtained (data not shown), if we plot the plateau unfolding rate constant (the value of k_{obs} reached at high SDS concentrations after k_{max} starts to decline) versus SDS mole fraction. Further, the SDS concentration at which k_{max} occurs increases linearly with SDS mole fraction and also increases with log k_{max} (insert to Figure 8B). Put simply, as we increase the mole fraction of SDS, we also increase the concentration range over which the unfolding rate constant can increase, and consequently, we can reach a higher k_{max}.

Although there are only data points for four different mole fractions of SDS in Figure 8B, the individual points are determined with great reliability based on an extensive series of measurements in Figure 8A. It is clear that the correlation between SDS mole fraction and log k_{max} is not linear, but rather hyperbolic. It is interesting to speculate about the basis of this type of correlation. Pioneering work by Bowie and co-workers on the equilibrium denaturation of membrane proteins such as diacyl glycerate kinase[35] and bacteriorhodopsin[36] in mixed micelles of SDS and DDM suggest a simple linear correlation between SDS mole fraction and the free energy of unfolding. This correlation can be transferred to the analysis of the kinetics of unfolding (where the activation energy of unfolding is proportional to log k of unfolding), as has been shown by ourselves[37,38] and Booth and co-workers.[39] Such a correlation may be rationalized by the fact that membrane proteins have well-defined binding sites for surfactant micelles, defined by the hydrophobic belt of amino acids that is inserted into the membrane. Therefore mixed micelles can be expected to bind to the native state in much the same way irrespective of their composition, justifying a straightforward comparison between micelles with different SDS compositions. Any change in stability or unfolding kinetics will reflect the impact of an altered amount of SDS "seen" by the protein within the micelle, without having to invoke any micellar rearrangements. In contrast, there are no intrinsic predefined micellar binding sites on globular proteins such as ACBP, and therefore, it is likely that as we alter the micellar composition we will also alter the relative

micelle-binding affinities of different regions of ACBP. This will affect the whole denaturation process and is the most likely reason for the deviation from a simple linear relationship that we observe in Figure 8B. Micelles containing only DDM do not interact at all with ACBP, and therefore, increases in SDS contents at low SDS mole fractions will lead to a series of micelles with a steeply increasing affinity for ACBP and with an opportunity to sample many different binding sites. Above a certain mole fraction of SDS, however, we suggest that the impact of changing SDS contents will not lead to significantly altered binding sites. This will lead to a more modest increase in unfolding rate with increasing SDS mole fraction. Although we predict that the same hyperbolic relationship seen in Figure 8B will be observed for other globular proteins, it is very likely that the sequence and structure of the protein in question, and thus, the potential binding sites for micelles will affect the specific shape of the hyperbolic curve.

Note that these reflections base themselves solely on our kinetic measurements. Our equilibrium measurements for the first transition of unfolding in mixed micelles (Figure 3) do not show such a dramatic variation in denaturation properties with changing mole fractions (data for neat SDS cannot be included as SDS does not form micelles during the first denaturation transition), indicating that differences between mixed micelles are mainly a question of how they initially "attack" and denature ACBP. As well as highlighting the usefulness of kinetic data for differentiating micelle effects, this also re-emphasizes the difference between globular proteins and membrane proteins, since equilibrium denaturation is a highly informative analytical approach for the latter.[36]

Power-Law Rise Based on Weak Protein−Surfactant Interactions. Interestingly, the kinetics of unfolding in micelles containing 25% SDS show the same power-law rise at higher surfactant concentrations as we observe for C8-alkyl sulfates. In both cases, the unfolding rate constant, from which the power-law rise starts out, is very low. This suggests a very high activation barrier which can be reduced by micellar changes occurring at high surfactant concentrations. It is remarkable that these kinetic phenomena are induced by micelles which reduce affinity toward ACBP by two very different means, namely by weakening either hydrophobic or electrostatic interactions. In both cases, we see that when an attractive interaction is weakened (as indicated by a low unfolding rate constant), other modes of binding can more easily manifest themselves at higher surfactant concentrations. This indicates that both hydrophobicity and electrostatics are central for interactions between micelles and proteins.

More insight into these processes can be obtained by coplotting k_{obs}, the amplitude, and the end-point of the unfolding reaction versus surfactant concentration for the 25% SDS data (Figure 8C). The amplitude is the difference in fluorescence between the start and end point of the reaction we monitor in our stopped-flow apparatus and thus provides an indirect measure of the degree of structural change associated with unfolding, as well as the degree to which this reaction goes to completion. At low concentrations of SDS (up to 5 mM), the amplitude and end-point increase to a plateau level in parallel with k_{obs}, reflecting the fact that more and more of the protein unfolds as we increase SDS concentration (cf. Figure 3A). As we increase the SDS concentration from 5 to ~50 mM, both k_{obs} and the amplitude decrease while the end point remains relatively constant. This can be rationalized as the gradual accumulation of a different type of micelle over this concentration range, which binds to ACBP in a different manner at the beginning of the unfolding reaction (leading to an altered initial fluorescence level), although the end state is relatively unaffected. We have used the acridine orange fluorescence assay reported by Romani et al.[30] to determine the concentration cmc_2 at which elongated micelles appear in these mixed micelles (Figure 8D). This occurs around 10−12 mM SDS which corresponds nicely to the decline in unfolding rate constants and suggests that the elongated micelles are also responsible for decreasing rate, even when the proportion of SDS has decreased to a very modest level. It is only as we increase the concentration of SDS_{total} above ~60 mM, and the k_{obs} values start to rise, that the end species starts to change in fluorescence, while the amplitude now remains relatively constant. This indicates that it is now the end species, rather than the starting species, that is changed by the altered surfactant concentration.

Similar correlations between unfolding rate constants, amplitudes, and end point values can be observed for unfolding of ACBP in C8-sulfate (data not shown). These data provide an indication of the many subtle changes that occur in protein−surfactant interactions with increasing surfactant concentration.

Summary

We undertook this study to explore the correlation between alkyl chain length, micellar charge, and denaturation potency toward the protein ACBP. As expected, alkyl sulfates with longer chain lengths and lower cmc values denature ACBP at lower concentrations than the shorter chains; in addition, they also generally give rise to faster denaturation kinetics. However, below cmc all surfactants show the same linear correlation between log k_{unf} and surfactant concentration with slopes that correlate with chain length, indicating a fundamentally similar denaturation mechanism in this range. This linear increase in unfolding rates by monomeric surfactants is halted by the formation of micelles which lead to a marked decrease in unfolding rates. For SDS, the decline only occurs at concentrations well above cmc and may be attributed to the formation of rodlike micelles with weaker binding affinity as well as the ability to bind to ACBP in multiple modes, some of which can slow down unfolding. We observe that the decline already starts at the cmc in the case of shorter chain length micelles, suggesting that these micelles have a weaker binding affinity from the beginning. Diluting out SDS with nonionic surfactants makes the transition to rodlike micelles occur at lower concentrations and also brings on an earlier decline in the unfolding rate constant. For both short-chain surfactants and mixed micelles with reduced charge, the very low unfolding rates give way to a power-law increase in unfolding rates at higher surfactant concentrations which we attribute to the existence of high activation barriers that allow alternative binding sites on the protein surface to emerge. Furthermore, the nonlinear response of unfolding rate constants to SDS mole fractions suggests the existence of a range of different binding regions on the ACBP surface, depending on the SDS mole fraction.

Abbreviations: ACBP, acyl coenzyme A binding protein; DDM, dodecyl maltoside; C*X*-sulfate ($X = 8-16$), sodium alkyl sulfate where the alkyl chain contains 8−16 carbon chains.

Acknowledgment. K.K.A. is supported by Aalborg University and by a stipend provided by the innovation consortium BIOPRO, financed by the Danish Ministry of Science, Innovation and Technology. We thank Professor Peter Westh, Professor Jan Skov Pedersen, and Dr. Cristiano Oliveiro as well as Dr. Torben Madsen for general discussions about protein−surfactant interactions and Professor Flemming M. Poulsen for generously providing purified ACBP mutants.

References and Notes

(1) Putnam, F. W. *Adv. Protein Chem.* **1948**, *4*, 79.
(2) Randolph, T. W.; Jones, L. S. *Pharm. Biotechnol.* **2002**, *13*, 159.
(3) Otzen, D. E.; Oliveberg, M. *J. Mol. Biol.* **2002**, *315*, 1231.
(4) Stoner, M. R.; Dale, D. A.; GUalfetti, P. J.; Becker, T.; Randolph, T. W. *Biotechnol. Prog.* **2006**, *22*, 225.
(5) Lu, R. C.; Cao, A. N.; Lai, L. H.; Zhu, B. Y.; Zhao, G. X.; Xiao, J. X. *Colloid Interface B. Biosurf.* **2005**, *41*, 139.
(6) Columbus, L.; Lipfert, J.; Jambunathan, K.; Fox, D. A.; Sim, A. Y.; Doniach, S.; Lesley, S. A. *J. Am. Chem. Soc.* **2009**, *131*, 7320.
(7) Hilty, C.; Wider, G.; Fernández, C.; Wüthrich, K. *Chembiochem* **2004**, *5*, 467.
(8) Timmins, P.; Pebay-Peyroula, E.; Welte, W. *Biophys. Chem.* **1994**, *53*, 27.
(9) Cunningham, E. L.; Jaswal, S. S.; Sohl, J. L.; Agard, D. A. *Proc. Natl. Acad. Sci. USA* **1999**, *96*, 11008.
(10) Kragelund, B. B.; Poulsen, K.; Andersen, K. V.; Baldursson, T.; Kroll, J. B.; Neergard, T. B.; Jepsen, J.; Roepstorff, P.; Kristiansen, K.; Poulsen, F. M.; Knudsen, J. *Biochemistry* **1999**, *38*, 2386.
(11) Kragelund, B. B.; Robinson, C. V.; Knudsen, J.; Dobson, C. M.; Poulsen, F. M. *Biochemistry* **1995**, *34*, 7217.
(12) Nielsen, M. M.; Andersen, K. K.; Westh, P.; Otzen, D. E. *Biophys. J.* **2007**, *92*, 3674.
(13) Otzen, D. E. *Biophys. J.* **2002**, *83*, 2219.
(14) Otzen, D. E.; Nesgaard, L.; Andersen, K. K.; Hansen, J. H.; Christiansen, G.; Doe, H.; Sehgal, P. *Biochim. Biophys. Acta* **2008**, *1784*, 400.
(15) Andersen, K.; Westh, P.; Otzen, D. E. *Langmuir* **2008**, *15*, 399.
(16) Manning, M.; Colón, W. *Biochemistry* **2004**, *43*, 11248.
(17) Andersen, K. K.; Oliveira, C. L. P.; Larsen, K. L.; Poulsen, F. M.; Callisen, T. H.; Westh, P.; Pedersen, J. S.; Otzen, D. E. *J. Mol. Biol.* **2009**, *391*, 207.
(18) Mandrup, S.; Hojrup, P.; Kristiansen, K.; Knudsen, J. *Biochem. J.* **1991**, *276* (Pt 3), 817.
(19) Kalyanasundaram, K.; Thomas, J. K. *J. Am. Chem. Soc.* **1976**, *99: 7*, 2039.
(20) Pace, C. N. *Methods Enzymol.* **1986**, *131*, 266.
(21) Nielsen, M. M.; Andersen, K. K.; Westh, P.; Otzen, D. E *Biophys. J.* **2007**, *92*, 3674.
(22) Vass, S. *Struct. Chem.* **1991**, *2* (167)), 375.
(23) Otzen, D. E.; Sehgal, P.; Westh, P. *J. Colloid Interface Sci.*, in press.
(24) Sehgal, P.; Mogensen, J. E.; Otzen, D. E. *Biochim. Biophys. Acta* **2005**, *1716*, 59.
(25) Otzen, D. E *Biophys. J.* **2002**, *83*, 2219.
(26) Mogensen, J. E.; Ibsen, H.; Lund, J.; Otzen, D. E. *Biochemistry* **2004**, *43*, 3357.
(27) Kragelund, B. B.; Robinson, C. V.; Knudsen, V.; Dobson, C. M.; Poulsen, F. M. *Biochemistry* **1995**, *34*, 7217.
(28) Croonen, Y.; Geladé, E.; Van der Zegel, M.; Van der Auweraer, M.; Vandendriessche, H.; De Schryver, F. C.; Almgren, M. *J. Phys. Chem.* **1983**, *87*, 1426.
(29) Clint, J. H. *Surfactant aggregation*; Chapman & Hall: New York, 1992.
(30) Romani, A. P.; da Hora Machado, A. E.; Hioka, N.; Severino, D.; Baptista, M. S.; Codognoto, L.; Rodrigues, M. R.; de Oliveira, H. P. *J. Fluoresc.* **2008**.
(31) Stoner, M. R.; Dale, D. A.; Gualfetti, P. J.; Becker, T.; Randolph, T. W. *Biotechnol. Prog.* **2006**, *22*, 225.
(32) Kragelund, B. B.; Osmark, P.; Neergaard, T. B.; Schiødt, J.; Kristensen, K.; Knudsen, J.; Poulsen, F. M. *Nat. Struct. Biol.* **1999**, *6*, 594.
(33) Kragelund, B. B.; Knudsen, J.; Poulsen, F. M. *J. Mol. Biol.* **1995**, *250*, 695.
(34) Kragelund, B. B.; Andersen, K. V.; Madsen, J. C.; Knudsen, J.; Poulsen, F. M. *J. Mol. Biol.* **1993**, *230*, 1260.
(35) Lau, F. W.; Bowie, J. U. *Biochemistry* **1997**, *36*, 5884.
(36) Faham, S.; Yang, D.; Bare, E.; Yohannan, S.; Whitelegge, J. P.; Bowie, J. U. *J. Mol. Biol.* **2004**, *335*, 297.
(37) Otzen, D. E. *J. Mol. Biol.* **2003**, *330*, 641.
(38) Sehgal, P.; Otzen, D. E. *Protein Sci.* **2006**, *15*, 890.
(39) Curnow, P.; Booth, P. J *Proc. Natl. Acad. Sci. USA* **2007**, *104*, 18970.
(40) Kragelund, B. B.; Osmark, P.; Neergaard, T. B.; Schiodt, J.; Kristiansen, K.; Knudsen, J.; Poulsen, F. M. *Nat. Struct. Biol.* **1999**, *6*, 594.

JP905553H